Journal of Molecular Liquids 341 (2021) 117405

Contents lists available at ScienceDirect

Journal of Molecular Liquids

journal homepage: www.elsevier.com/locate/molliq

Molecular collisions or resonance energy transfer in lipid vesicles? A methodology to tackle this question

Cássia A. Marquezin [a,*], M. Teresa Lamy [b], Eduardo S. de Souza [c]

[a] Instituto de Física, Universidade Federal de Goiás, CP 131, CEP 74001-970, Goiânia, GO, Brazil
[b] Instituto de Física, Universidade de São Paulo, Rua do Matão, 1371, CEP 05508-090, São Paulo, SP, Brazil
[c] Instituto de Física, Universidade Federal de Catalão, Av. Dr. Lamartine Pinto de Avelar, 1120, CEP 75704-020, Catalão, GO, Brazil

ARTICLE INFO

Article history:
Received 29 June 2021
Revised 20 August 2021
Accepted 26 August 2021
Available online 28 August 2021

Keywords:
FRET
Stern-Volmer
Fluorescence
Laurdan
Thiosemicarbazone
DMPC vesicles

ABSTRACT

In this work, molecular interactions in a lipid membrane are discussed through fluorescence spectroscopy data, both experimentally and theoretically. In particular, the fluorescence quenching mechanisms between the fluorescent probe *6-dodecanoyl-2-dimethylaminonaphthalene* (Laurdan) and the potential drug *2-nitrobenzaldehyde-thiosemicarbazone* (2-TSC) were studied, both inserted in a *1,2-dipalmitoyl-sn-glycero-3-phosphocholine* (DMPC) model membrane. The fluorescence intensity and the lifetime of Laurdan decrease dramatically in the presence of 2-TSC, in both gel and fluid phases of the DMPC bilayer. It is shown here how to identify the correct quenching mechanism, by conducting a careful analysis of the fluorescence data. The analysis of the bimolecular constant values obtained through the Stern-Volmer equation, considering the collisional mechanism, made clear the incompatibility of the obtained values with estimated diffusion coefficients for Laurdan and 2-TSC inserted into lipid bilayers. On the other hand, using the Förster's theory of resonance energy transfer (FRET) we obtained results in good agreement with the already known dynamic characteristics of a DMPC bilayer, at its both gel and fluid phases. Through spectroscopy data and computational calculation, Förster distance, energy transfer efficiency and distance distribution were obtained for the donor/acceptor pair Laurdan/2-TSC, at both gel and fluid phases of the bilayer. The distance distribution reflects the occurrence of FRET involving donor/acceptor pairs in the same leaflet of the lipid bilayer and pairs in opposite leaflet, and these results are in good agreement with our previous proposal about the lateral organization and position of Laurdan and 2-TSC molecules in a DMPC bilayer. All these results lead us to conclude that FRET between the donor Laurdan and the acceptor 2-TSC is the mechanism responsible for non-radiative deexcitation of Laurdan. The methodology used here could be extended to other pairs of donor/acceptor molecules, to contribute to the knowledge about their localizations in lipid membranes.

1. Introduction

Techniques based on fluorescence microscopy and fluorescence spectroscopy have been intensively employed in biophysics, allowing the study of a wide variety of biologically relevant molecules. Advanced techniques in fluorescence microscopy [1] allow the acquisition of bioimages [2,3], through which it is possible to study, for example, macromolecular fluxes in capillaries *in vitro* [4] and even *in vivo* [5,6] systems. On the other hand, fluorescence spectroscopy, both steady state and time resolved, have been widely used to monitor molecular interactions [7–9]. In particular, some processes that decrease the fluorescence intensity and/or the fluorescence lifetime provide information about the proximity between molecules, or even inter and intramolecular distances, as Förster resonance energy transfer (FRET or RET) process [10,11]. Other processes that decrease the fluorescence intensity of a fluorophore are dynamic (or collisional) and static quenching. For collisional quenching to occur, the distance between molecules must be equal (or less) to their van der Waals radii [12,13], i.e., fluorophore and quencher have to come into molecular contact, allowing the electronic clouds of both molecules to interact. On the other hand, FRET does not require contact between molecules, and can occur at distances up to ~100 Å, according to Förster's theory [14] of non-radiative energy transfer via dipole–dipole interaction. For the resonance energy transfer to occur, the spectral overlap between the emission spectrum of the donor molecule and the optical absorption spectrum of the acceptor molecule is necessary.

* Corresponding author.
E-mail address: cassia_m@ufg.br (C.A. Marquezin).

https://doi.org/10.1016/j.molliq.2021.117405
0167-7322/

Both mechanisms, collisional quenching and FRET, have become tools that are widely used in a variety of applications. FRET, for instance, has been applied to studies with fluorescent biosensors [15–17], supramolecular systems [18–21], nucleic acids [22–25] and polypeptides [26–29]. FRET has also been applied to studies of model membranes [30–32], where it is used to monitor the location and the distribution of molecules in phospholipid bilayers [33–36].

The collisional quenching mechanism is well described by the Stern-Volmer model, widely employed in studies that can reveal the location of molecules inserted in macromolecular systems through the accessibility of the fluorophores to a quencher [37–42]. This accessibility can be monitored by the bimolecular quenching constant k_q, which reveals the association/binding behavior between fluorophore and quencher.

However, in some cases where there is both the decrease of the fluorescence intensity and lifetime of a fluorophore in the presence of another molecule, and there is some spectral overlap, it is not obvious to affirm whether FRET or collisional quenching occurs. Both, the collisional quenching and FRET, are processes that decrease the fluorescence intensity and the lifetime of the fluorophore, because these processes depopulate the excited state. Consequently, a comparison between the two processes must be carefully conducted to completely understand which mechanism is responsible for the decrease in the fluorescence signal, and to be able to draw conclusions about the distance between them, and, possibly, their localization in a membrane.

In a previous work [43] we noticed that the presence of the potential drug *2-nitrobenzaldehyde-thiosemicarbazone* (2-TSC) [44], derived from a terpene [45,46], caused a decrease in the fluorescence intensity and lifetime of the well know fluorescent probe *6-dodecanoyl-2-dimethylaminonaphthalene* (Laurdan) [47–53], both molecules inserted into *1,2-dipalmitoyl*-sn-*glycero-3-phosphocholine* (DMPC) bilayer. DMPC vesicles are among the most common model systems for studying the location, behavior, permeability and antioxidant properties of different types of drugs in membranes. This model is an effective tool for understanding molecular-level processes, which is the focus of this work. The 2-TSC molecule was found to show antitumor activity against human tumor cell lines [44] as is typical for thiosemicarbazones [54] and, despite its aromaticity, displays no fluorescence [43]. As Laurdan is known to be localized close to the membrane surface [55,56], and considering collisional quenching between 2-TSC and Laurdan, it was concluded that this should also be the location of 2-TSC in the lipid membrane. However, it was mentioned that the possibility of FRET between the two molecules could not be ruled out, although the spectral overlap between the Laurdan emission and the optical absorption of 2-TSC was found to be relatively small.

In the present work, we revisit the interaction between 2-TSC and Laurdan, analyzing the fluorescence data using both methods, collisional quenching and FRET. By analyzing the bimolecular quenching constants obtained, the fluorescence lifetime of Laurdan in DMPC bilayers and the lateral diffusion coefficient of the molecules involved, we concluded that the collisional quenching mechanism was not the process that causes the decrease of fluorescence intensity and lifetime of Laurdan. On the other hand, it was possible to show that the decrease in the fluorescence signal of Laurdan was most likely due to FRET to the acceptor 2-TSC, and the Förster distance R_0 and the energy transfer efficiency E for this donor/acceptor pair were obtained for the molecules in DMPC membranes, at both gel and fluid phases. We also recovered distance distributions between Laurdan and 2-TSC by using a modified version of the open source CONTIN program [57], that inverts general systems of linear algebraic equations, as presented in our previous works [26–28,36]. The methodology developed in this work, to elucidate which type of molecular interaction is occurring when a decrease in fluorescence is observed, can also be extended to pairs of molecules inserted in biological membranes. Despite the complex composition of biological membranes, the analysis of fluorescence intensity decays, together with the calculation of donor and acceptor diffusion coefficients, allows the correct identification of the mechanism responsible for the decrease of the fluorescence intensity and lifetime.

2. Materials and methods

2.1. Samples

2-nitrobenzaldehyde-thiosemicarbazone (2-TSC) was prepared as previously described [44]. *6-dodecanoyl-2-dimethylaminonaphthalene* (Laurdan) was purchased from Molecular Probes Inc. (Eugene, OR, USA). The phospholipid *1,2-dimyristoyl-sn-glycero-3-phosphocholine* (DMPC) was supplied by Avanti Polar Lipids Inc. (Birmingham, AL, USA). *4-(2-hydroxyethyl)-1-piperazineethanesulfonic acid* (HEPES) was purchased from Sigma Aldrich (St Louis, MO). All compounds were used without further purification. Milli-Q Plus water (Millipore), pH ~ 6, was used for buffer preparation. Measurements in aqueous medium were performed in HEPES buffer 10 mM, pH 7.4. Fig. 1 shows the chemical structures of the acceptor 2-TSC and the donor Laurdan.

2.2. Preparation of vesicles

Vesicles were obtained from the extrusion method [58]. Briefly, 1 mM of lipid was dissolved in chloroform. The sample was dried with nitrogen and the solvent completely removed under reduced pressure to obtain the dried lipid film. The lipid films were hydrated in buffer solution (HEPES 10 mM pH 7.4) to obtain a 1 mM lipid concentration and vortexed. The suspension was than extruded 21 times through polycarbonate membranes, using a Mini Extruder from Avanti Polar Lipids Inc. (Birmingham, AL, USA). The extrusion was made using 0.1 μm pore diameter polycarbonate membranes (from Millipore), resulting in a population of monodisperse Large Unilamellar Vesicles (LUV), with average diameter of 0.1 μm.

For spectroscopic measurements, the fluorophore Laurdan was added to the lipid/chloroform solution at 1 mol% of the lipid concentration. All experiments were performed in the absence and presence of three different 2-TSC concentrations (1, 5 and 10 mol

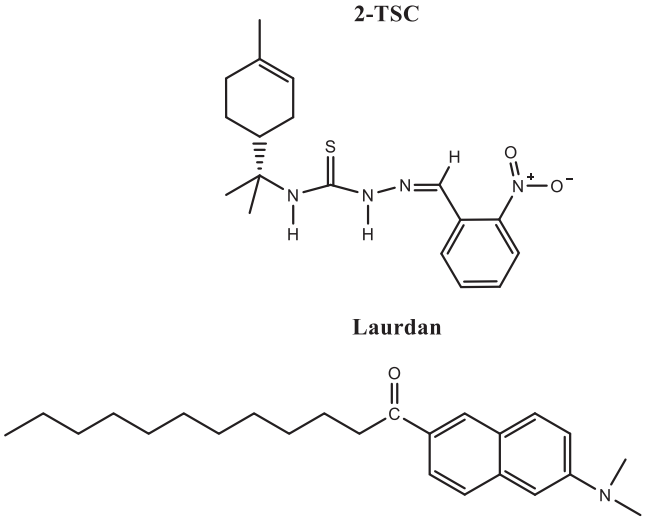

Fig. 1. Molecular structures of the compounds studied in this work.

% of the lipid concentration). 2-TSC was also mixed with the lipid/chloroform solution.

2.3. Methods

Optical absorption spectra were obtained with an UV−Vis spectrophotometer (Varian Cary, Santa Clara, CA). Samples were placed in quartz cuvettes, with absorption optical pathway of 2 mm. The temperature was controlled with a Carry Peltier thermostat. To ensure thermal equilibrium, before each scan the sample was left at the desired temperature for at least 10 min.

For steady state fluorescence spectroscopy, samples were placed in quartz cuvettes with 2 mm optical pathway. Measurements were performed using the Varian Cary Eclipse spectrofluorometer. The temperature was controlled by a Peltier system. To ensure thermal equilibrium, before each scan the sample was left at the desired temperature for at least 10 min. Emission spectra were measured with excitation wavelength at 330 nm for Laurdan, used here as a fluorescent membrane probe.

Time-resolved fluorescence measurements were performed using the time-correlated single photon counting method (TCSPC) [12]. The excitation source used was a titanium-sapphire laser Tsunami 3950 from Spectra Physics, pumped by a solid-state laser Millenia Pro model J80, also from Spectra Physics. The repetition rate was set to 8000 kHz using a pulse picker (Spectra Physics, model 3980-25). The Tsunami was set to give an output of 990 nm and a third harmonic generator BBO crystal (GWN-23PL Spectra Physics) was used to generate the excitation beam at 330 nm. This beam was directed to a spectrofluorometer from Edinburgh (FL900CDT). The emitted light was detected at 90° from the excitation beam. The emission wavelength was selected by a monochromator and the emitted photons were detected by a refrigerated microchannel plate photomultiplier (Hamamatsu R3809U). The FWHM of the instrument response function was 90–110 ps. Time resolution was 12 ps per channel. The temperature was controlled within 0.1 °C by the thermal bath Julabo HP 25. Excitation wavelength was at 330 nm, and the emission detected at 480 nm.

Software from Edinburgh Instruments was used to analyze the decay curves. The intensity decays were fitted to the equation [12]:

$$I(t) = \sum_i \alpha_i e^{-t/\tau i} \tag{1}$$

where τ_i is the lifetime of the i^{th} component of the decay, and α_i is the corresponding pre-exponential factor. The quality of fit was judged by statistical parameters like reduced χ^2 and by plot of residuals.

2.4. FRET theory

According to Förster's theory [14] of non-radiative energy transfer via dipole–dipole interaction, for a single fixed distance, r, between donor and acceptor, the FRET rate (k_T) is [12]:

$$k_T = \frac{1}{\tau_d}\left(\frac{R_0}{r}\right)^6 \tag{2}$$

where R_0 is the Förster distance and τ_d is the excited state lifetime of donor molecule (single exponential decay) in the absence of acceptor. The Förster distance is given by:

$$R_0^6 = \frac{9000(ln10)\kappa^2\phi_d}{128\pi^5 n^4 N_0} J \tag{3}$$

where ϕ_d is the donor quantum yield in the absence of acceptor, n is the index of refraction of the medium, N_0 it the Avogadro number, J is the spectral overlap integral and κ^2 is the orientation factor. The orientation factor depends on the relative orientation of transition dipole moments of the donor and acceptor. The overlap integral is given by:

$$J = \int F_d(\lambda)\varepsilon_a(\lambda)\lambda^4 d\lambda \tag{4}$$

where F_d is the area-normalized donor fluorescence spectrum in the absence of the acceptor and ε_a is the molar absorptivity of the acceptor.

The experimental FRET efficiency can be calculated by [12]

$$E = 1 - \frac{\int_0^\infty I_{da}(t)dt}{\int_0^\infty I_d(t)dt} \tag{5}$$

where I_d and I_{da} are the measured donor intensity decay profile in the absence and presence of the acceptor, respectively.

2.5. Computation - FRET distance distribution in lipid membranes

In this work we considered a population of donor–acceptor pairs in a phospholipid bilayer with different distances from each other that lead to a distance distribution function, $f(r)$. Donor-acceptor pairs, separated by the distance r, contribute to the measured fluorescence intensity through $f(r)$. The fluorescence intensity decay of donor in the absence of acceptor, in the case of complex decay, is $I_d(t) = \sum_i \alpha_i exp\left(-\frac{t}{\tau_{di}}\right)$. In the presence of the acceptor, the FRET additional route for deexcitation (k_T)affects the fluorescence decay of the donor. The total fluorescence intensity decay of donor in the presence of acceptor, $I_{da}(t)$, integrated over the distance distribution, is given by [26,28,59,60]:

$$I_{da}(t) = \int_a^b f(r)\cdot I_d(t)\cdot exp\left[-\left(\frac{R_0}{r}\right)^6 \frac{t}{\langle\tau\rangle}\right] dr \tag{6}$$

where $\langle\tau\rangle = \frac{\sum_i \alpha_i \tau_i}{\sum_i \alpha_i}$ is the amplitude-averaged lifetime, a and b the range of distances for the system. The distance distribution can be recovered by fitting Eq. (6) to the experimental decay curve.

The fitting of Eq. (6) was done using the open source CONTIN program [57] that inverts general systems of linear algebraic equations of the type

$$y(t_k) = \int_a^b s(x)K(x,t_k)dx + \sum_{j=1}^{N_L} L_j(t_k)\beta_j \tag{7}$$

In this work, $y(t_k)$ corresponds to the measured intensity of fluorescence $I_{da}(t_k)$, at the instant t_k; x is the donor–acceptor distance relative to the Förster distance, i.e., $x = r/R_0$; $K(x,t_k)$ is a known function to describe the intensity decay with the occurrence of energy transfer and $s(x)$ is the distance distribution function to be recovered by the program. The second term can be used for corrections like the background or impurities that may be present and contributing to the decay profile. The integral is converted, by numerical integration, to a summation in x_j.

To the fitting of Eq. (6) we modified CONTIN code by considering $s(x)$ the distance distribution function $f(x)$ and defining

$$K(x,t_k) = \int_0^t L(t')I_d(t-t')\cdot exp\left[-x^6\frac{(t-t')}{\langle\tau\rangle}\right] \tag{8}$$

where L is the instrument response function. Due to the strong dependence of FRET efficiency on the donor–acceptor distance, the range of relative distances was restricted from $0.5R_0$ to $2R_0$ [12]. This range, set in the input file, is divided in N equally spaced intervals. The distance distribution is recovered using the weighted least squares method with the employment of a regularizor based on the principle of parsimony [57]. In the analysis, we also imposed the constraint of non-negativity for the distribution function.

2.6. Stern-Volmer equation

The Stern-Volmer equation, that describes collisional quenching mechanisms, is giving by:

$$\frac{F_0}{F} = \frac{\tau_0}{\tau} = 1 + k_q \tau_0 [Q] \quad (9)$$

where F_0 and τ_0 are the fluorescence intensity and fluorescence lifetime of the fluorophore in the absence of the quencher, respectively, *[Q]* is the molar concentration of the quencher and k_q is the bimolecular quenching constant.

All data shown here are means of at least two experiments, and the uncertainties are the standard deviations.

3. Results and discussion

The emission spectrum of Laurdan exhibits dramatic red shift when the probe is inserted in a phospholipid bilayer that undergoes gel to fluid phase transition. Rowe and Neal analyzed the fluorescence decay data of Laurdan inserted into DMPC bilayer. The data were arranged in the form of Fourier transformed emission-decay matrices, by methods based on principal components analysis [61]. They found clear evidence that Laurdan presents, at least, three emissive states, which they called locally excited, charge-transfer and solvent relaxed states, all of them with excited state interactions with each other. However, the explanation of the Laurdan red shift upon bilayer phase transition is still under debate. Vequi-Suplicy et al. [62] proposed that two emission bands of Laurdan, in homogeneous solvents, would be related to the emission of two independent states, and not to a pair of non-relaxed and solvent relaxed states. The investigation was conducted in solvents of different polarities by time-resolved fluorescence, decay associated spectra and Gaussian decomposition of the fluorescence emission spectrum. More recently, Vequi-Suplicy et al., using a sequential hybrid Quantum Mechanics/Molecular Mechanics method, brought support for the hypothesis that the fluorescent emission of Prodan, in several solvents, occurs from two independent excited states, and argued that the same reasoning may explain the dual band fluorescence of Laurdan [63].

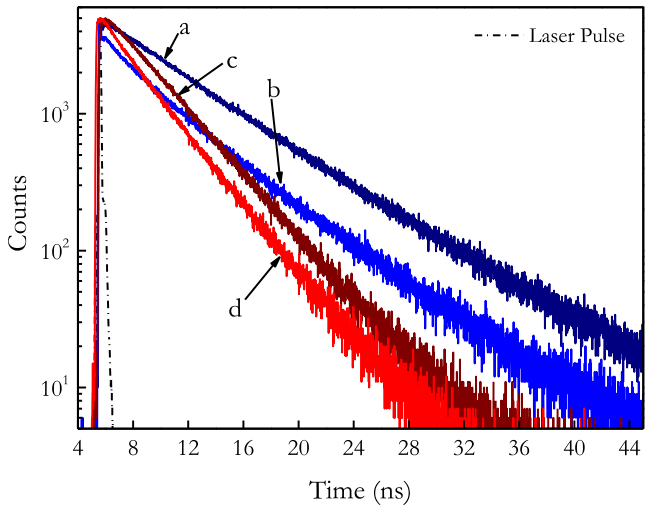

Fig. 2. Typical fluorescence intensity decays of Laurdan in DMPC, at the bilayer gel phase (15 °C) in the (a) absence and in the (b) presence of 1 mol % of 2-TSC, and at the fluid phase (35 °C) in the (c) absence and in the (d) presence of 1 mol % of 2-TSC. Excitation wavelength was at 330 nm, and emission was detected at 480 nm.

The contribution of the excited states to the total fluorescence of Laurdan could be obtained by the decomposition of its emission spectrum into two Gaussian bands. The blue band was associated to the peak centered at ~440 nm and the red band to the peak centered at ~490 nm [64]. These two bands were observed to different extents in both gel and fluid phases of phosphatidylcholine and phosphatidylglycerol membranes. However, at wavelengths greater than 480 nm, the contribution of the blue band is almost negligible at both gel and fluid bilayer phases [53,55,64,65].

In this work, we monitored the fluorescence of Laurdan inserted in a DMPC bilayer (phase transition temperature around 23 °C [66,67]) at 1 mol% of the lipid concentration. It was shown, by differential scanning calorimetry thermograms [43], that this concentration of Laurdan does not change the phase transition temperature of extruded 1 mM DMPC dispersions.

The intensity decay of Laurdan, measured at 480 nm, therefore related to the excited state associated to the red band, as discussed above, is strongly quenched upon gel to fluid phase transition of the DMPC (Fig. 2). The intensity-averaged lifetime of Laurdan into pure DMPC bilayer decreases from 6.8 ns in the gel phase to 3.7 ns in the fluid phase (Table 1). The relative areas of the red and blue bands obtained from Gaussian decomposition of the emission spectrum of the Laurdan in DMPC are, respectively, ~ 0.4 and ~0.6 in the gel phase and ~0.9 and ~0.1 in the fluid phase of the bilayer [65]. Therefore, the excited state associated to the red band is present in the gel and fluid phases of the bilayer while the excited state associated to the blue band is almost absent in the fluid phase.

With the addition of 1 mol% of 2-TSC (Fig. 2 and Table 1), a further decrease of the Laurdan intensity-averaged lifetime was

Table 1
Lifetimes and normalized pre-exponential factors obtained from fitting Laurdan intensity decay data to a multiexponential function. The data are for Laurdan in DMPC vesicles, before (15 °C) and after (35 °C) the bilayer gel-fluid phase transition, without and with different concentrations of 2-TSC. The average lifetime was obtained by $\langle\tau\rangle = \sum \alpha_i \tau_i^2 / \sum \alpha_i \tau_i$.

[2-TSC] mol%		0	1	5	10
τ_1 (ns)	15 °C	7.6 ± 0.5	5.5 ± 0.3	3.9 ± 0.2	3.1 ± 0.3
	35 °C	3.7 ± 0.1	3.5 ± 0.2	3.0 ± 0.2	2.5 ± 0.2
τ_2 (ns)	15 °C	5.2 ± 0.4	2.3 ± 0.4	1.4 ± 0.2	0.9 ± 0.1
	35 °C	–	1.6 ± 0.5	1.0 ± 0.2	0.8 ± 0.2
α_1	15 °C	0.58	0.73	0.56	0.32
	35 °C	1.00	0.82	0.66	0.54
α_2	15 °C	0.42	0.27	0.44	0.68
	35 °C	–	0.17	0.34	0.46
$\alpha_1\ \tau_1$ (ns)	15 °C	4.3 ± 0.3	4.0 ± 0.2	2.2 ± 0.1	1.0 ± 0.1
	35 °C	3.7 ± 0.1	2.9 ± 0.2	2.0 ± 0.1	1.3 ± 0.1
$\alpha_2\ \tau_2$ (ns)	15 °C	2.2 ± 0.2	0.6 ± 0.1	0.6 ± 0.1	0.6 ± 0.1
	35 °C	0.0 ± 0.0	0.3 ± 0.1	0.4 ± 0.1	0.4 ± 0.1
$\langle\tau\rangle$ (ns)	15 °C	6.8 ± 0.4	5.0 ± 0.3	3.3 ± 0.2	2.3 ± 0.3
	35 °C	3.7 ± 0.1	3.3 ± 0.2	2.7 ± 0.1	2.1 ± 0.1

observed at both phases of the bilayer. Accordingly, static quenching was discarded, and the quenching of Laurdan fluorescence by 2-TSC in a DMPC bilayer was supposed to be either a collisional quenching process or a FRET process in our previous work [43]. These two possibilities are deeper investigated in this work. It is important to mention that the fluorescence intensity of Laurdan was also found to decrease in the presence of 2-TSC [43].

3.1. Collisional quenching mechanism

In order to conduct a detailed comparative study between collisional quenching and FRET processes, we initially used the Stern-Volmer equation (Eq. (9)) to analyze the fluorescence data of Laurdan. By fitting the Stern-Volmer equation to the intensity-averaged decay lifetime of Laurdan (Table 1), in the absence and in the presence of 2-TSC, we obtained very large bimolecular quenching constants: $k_q = (3.0 \pm 0.3) \times 10^{12} s^{-1} M^{-1}$ and $k_q = (2.0 \pm 0.4) \times 10^{12} s^{-1} M^{-1}$, for the gel and fluid phases of DMPC, respectively (Fig. 3). Comparing with other examples of collisional quenching in membranes, these values of k_q are quite large. For instance, much larger than the bimolecular quenching constant of $(5.2 \pm 0.4) \times 10^{8} s^{-1} M^{-1}$ found for the quenching of 1,6-diphenyl-1,3,5-hexatriene (DPH) fluorescence by the acemetacin, both inserted in a DMPC bilayer at 37 °C [68]. They are even much larger than the one observed for the quenching of tryptophan by molecular oxygen in solution: 1.2×10^{10} $M^{-1}s^{-1}$ [69]. This would be, approximately, the largest possible value for k_q in aqueous solution, since other quenchers are much larger than the molecular oxygen and, consequently, have much lower diffusion coefficients.

To better understand these large values obtained for the bimolecular quenching constant, it is important to consider the Laurdan excited state lifetime, and the diffusion coefficients of molecules in a lipid bilayer. For instance, one could consider the longest lifetime component obtained for Laurdan in DMPC at the gel phase, 7.6 ns (Table 1). About diffusion movements in membranes, lateral diffusion coefficients of a DMPC molecule in the bilayer at the gel and fluid phases are 7 and 50 $\mu m^2 s^{-1}$, respectively [70]. Akhunzada *et al.* obtained the value of 12.2 $\mu m^2 s^{-1}$ for the lateral diffusion coefficient of Laurdan in DOPC giant unilamellar vesicles [71]. The root mean square distance diffused by the light excited probe can be calculated by $\sqrt{2D\tau}$, where D and τ are the diffusion coefficient and the excited state lifetime of the probe, respectively [12]. Thus, using the values of diffusion coefficient and lifetime of Laurdan presented above, we obtain ~4 Å as an estimative for the root mean square distance diffused by the excited molecule of Laurdan in DMPC. Therefore, the 2-TSC molecule should be at a distance shorter than 4 Å to be able to quench the Laurdan fluorescence by collision (molecular contact), which is not a reasonable distance for Laurdan and 2-TSC uniformly distributed in the lipid bilayer at the concentrations used in this work. Hence, the hypothesis of dynamic quenching of Laurdan by 2-TSC seems quite unlikely.

3.2. FRET mechanism

Considering that it does not seem to be reasonable to attribute the fluorescence quenching of Laurdan by 2-TSC to collisional quenching, the FRET mechanism was considered. The spectral overlap between Laurdan emission and 2-TSC optical absorption in DMPC vesicles, although visually small at first, results in a Förster distance appropriate for considerable FRET between this pair of molecules when the overlap integral J is calculated (Eq. (4)) from the absorption and normalized emission spectra (Fig. 4). The values of J (with wavelength in centimeters and molar absorption coefficient in $M^{-1}cm^{-1}$) obtained for the gel and fluid phases of the DMCP bilayer were 3.87×10^{-14} $M^{-1}cm^3$ and 3.12×10^{-14} $M^{-1}cm^3$, respectively. These are values that can be compared with values of J presented in previous works [26,60].

The Förster distance depends on the relative orientation of the donor and acceptor transition dipole moments, which is given by the kappa-squared term in Eq. (3). When the donor and the acceptor molecules are not highly constrained near-parallel to the membrane normal axis, the dynamic averaging regime can be considered [72], and in this regime, the value of the kappa-squared is 2/3. The choice of the dynamic averaging regime can also be upheld by analyzing the limiting anisotropy of the Laurdan. The limiting anisotropy is interpreted as resulting from an energy barrier that prevents rotational diffusion of the fluorophore beyond a certain angle [12]. If the fluorophore is not fully free to rotate, a non-zero limiting anisotropy manifests in the anisotropy decay. The limiting anisotropy of Laurdan in a DMPC bilayer goes from ~0.13 in the gel phase to zero in the fluid phase [47]. Lakowicz and Prendergast obtained a limiting anisotropy of ~0.3 for DPH in DMPC at gel phase [73]. Therefore, there is no rotational motion restriction of the Laurdan at the fluid phase of the DMPC bilayer and the restriction in the gel phase is smaller than that for the DPH in the same phase. The 2-TSC is not linked to a hydrocarbon tail and should not have a strong rotational motion restriction.

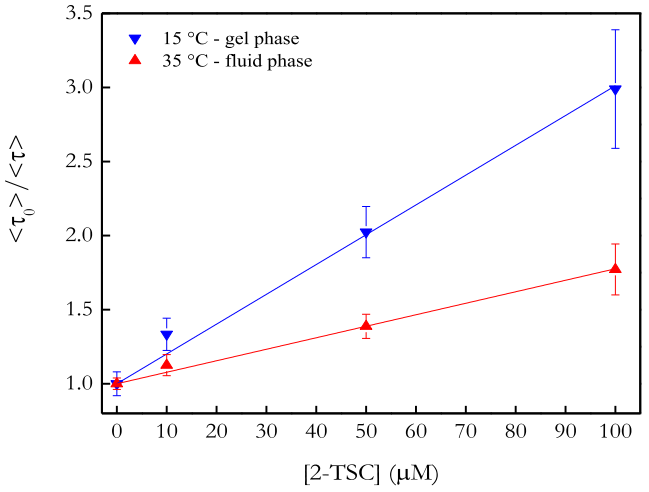

Fig. 3. Stern-Volmer plots: ratio of the intensity-averaged decay lifetime of Laurdan 1 mol% in DMPC 1 mM, in the absence ($\langle\tau_0\rangle$) and in the presence ($\langle\tau\rangle$) of 2-TSC.

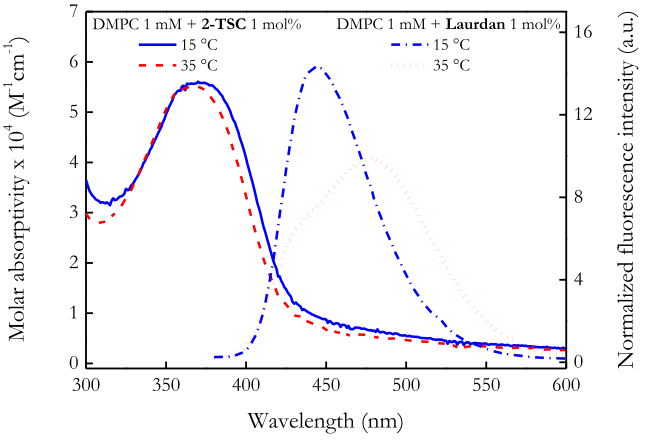

Fig. 4. Spectral overlap of 2-TSC (spectra on the left) extinction coefficient and Laurdan (spectra on the right) area-normalized fluorescence spectrum, both at 1 mol% in DMPC 1 mM at 15 °C (blue lines) and 35 °C (red lines).

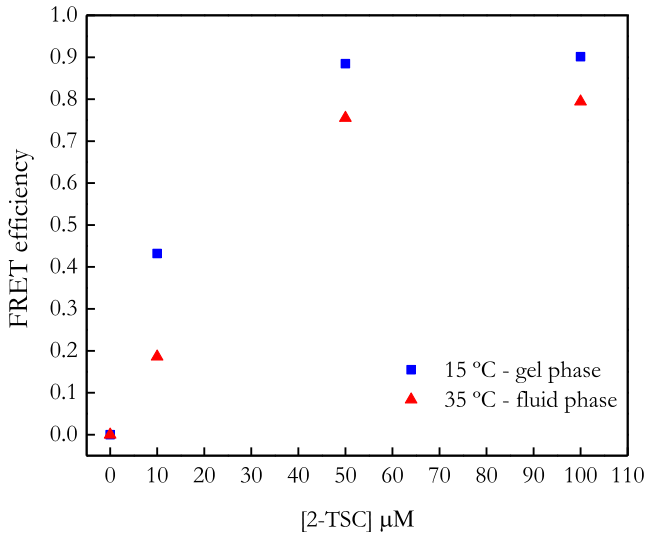

Fig. 5. FRET efficiency E for Laurdan/2-TSC pair in DMPC 1 mM vesicles at 15 °C (down triangle) and 35 °C (up triangle) as function of the molar concentration of the acceptor, calculated from Eq. (5).

Therefore, we considered the dynamic averaging regime for the calculation of the Förster distance in this work. In a study with controlled orientations of donor and acceptor transition moments, a change in the kappa-squared value from 0.476 to 0.801, associated with the transition from a disordered system to a moderately ordered system, respectively, resulted in an increase of only 9 % in Forster's distance [74]. Thus, the 2/3 value for kappa-squared used in this work would not significantly affect Förster's distance values.

The Förster distances R_0 (Eq. *(3)*) obtained for the gel and fluid phases were 37.2 Å and 35.9 Å, respectively. The Förster distance is the distance between the donor and the acceptor at which the transfer efficiency is exactly 50%. Moreover, we used the refractive index of the medium measured for a 1 mM of extruded DMPC dispersion, at room temperature (~25 °C), 1.331, and the Laurdan fluorescence quantum yield ϕ in DMPC vesicles (at 20 °C), 0.37 ± 0.01.

By using Eq. *(5)*, the FRET efficiency E between the donor Laurdan and the acceptor 2-TSC was obtained. Fig. 5 shows the efficiency as a function of acceptor molar concentration. The values of E are, interestingly, greater in the gel phase than in the fluid phase. However, the efficiency gives only an average information about the system. A more detailed information will be obtained by the distance distribution recovered from intensity decay fitting, as discussed below.

3.3. Distance distribution

The donor–acceptor distance distribution can be obtained by fitting Eq. (6) to the donor intensity decay data in the presence of the acceptor. In Eq. (6), it is considered that donor–acceptor distances can assume any value given the constraints of the system, and $f(r)$ is the contribution of a donor–acceptor pair separated by a distance r. A Gaussian function is generally assumed for the distance distribution [12]. In this work, the distance distribution was obtained without any *a priori* assumption concerning the shape of the distribution curves. The fitting of Eq. (6) was done using a modified version the open source CONTIN program [57]. The donor–acceptor distance distributions in both phases of the DMPC bilayer were recovered from the fluorescence decay data of Laurdan in the presence of 2-TSC molecules. The distance distribution presented three peaks for 2-TSC 1 mol% in DMPC vesicles, at both gel and fluid phases, as shown in Fig. 6.

We analyzed the distance distribution considering the two leaflets of the lipid bilayer. It is important to have in mind that both Laurdan and 2-TSC were mixed with the lipids in the bilayer preparation (see Materials and methods). Energy transfer between donor and acceptor located on the same leaflet is called *cis* transfer whereas energy transfer between donor and acceptor on opposite leaflets is called *trans* transfer. The thickness of the hydrated bilayer and the thickness of the hydrocarbon core of DMPC vesicles were considered to be 48 Å and 30 Å in the gel phase, and 44.2 Å and 26.2 Å in the fluid phase, respectively [75,76]. From the absorption spectrum of 2-TSC in water, ethanol and DMPC, it was proposed that the probe would be partially inserted in the region of the polar head groups or just below them [43]. Laurdan fluorescence quenching by Tempo-PCSL, in a DLPC bilayer, indicated that the fluorescence moiety of Laurdan would be localized close to the lipid bilayer surface [55]. Assuming these localizations for the pair Laurdan/2-TSC, the peak centered at ~23.5 Å (21.6 Å) can be associated to *cis* transfer in the gel (fluid) phase. The peak centered at ~39.1 Å (37.7 Å) in the gel (fluid) phase can be associated to *trans* transfer because these values of distance are between the bilayer hydrocarbon core thickness and hydrated bilayer thickness (Fig. 7).

The single photon counting (TCSPC) technic used here is a statistical method, with multiple cycles of excitation and emission to obtain the fluorescence decay profile. In each cycle, the excited donor can either emit a photon or transfer its energy to an acceptor. If a photon is emitted, the donor is not undergoing a non-radiative decay, therefore it means that there is no favorable acceptor within FRET distance range. Due to the dynamical aspect of the lipid bilayer, the closest acceptor of an excited donor in the TCSPC experiment can be further apart. Therefore, the peak centered at ~64.4 Å (55.7 Å) can be attributed to the far donor–acceptor pairs that undergo FRET.

The DMPC lipid diffusion coefficient is much smaller in the gel than in the fluid phase of the lipid bilayer [70]. This smaller lateral diffusion of molecules results in shorter distances displacement of the probes during excited state lifetime of the Laurdan in the gel phase of the bilayer. Thus, in the fluid phase, the longer displacement can lead an acceptor to the radius of action of an excited donor during its lifetime, allowing the occurrence of FRET. This process results in a broader long distance peak centered at shorter distance, in the distance distribution in the fluid phase, as showed in Fig. 6.

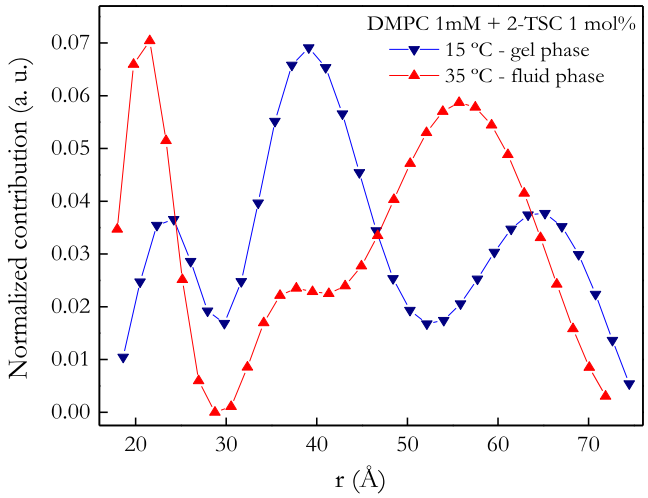

Fig. 6. Laurdan to 2-TSC 1 mol% distance distributions, obtained from fitting the FRET model to the Laurdan intensity decay data, in DMPC 1 mM at 15 °C (down triangle) and 35 °C (up triangle).

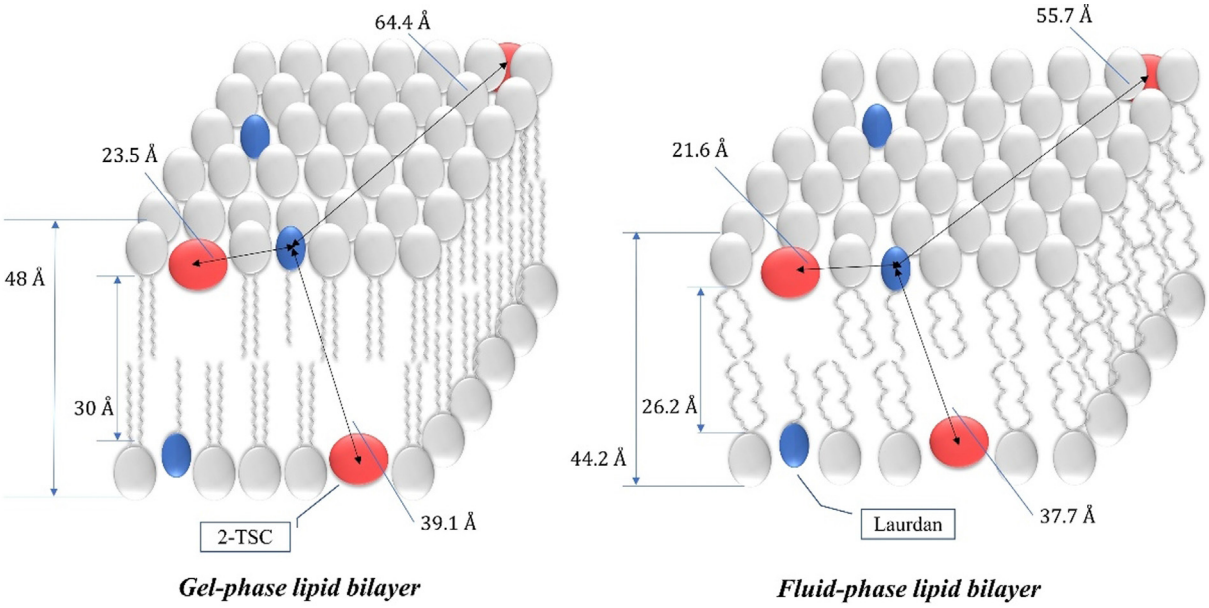

Fig. 7. A tentative diagram of the positions of Laurdan and 2-TSC molecules in a DMPC bilayer at gel (left) and fluid phases (right). The processes of *cis*-transfer and *trans*-transfer are illustrated as well the distances between the pair.

Still analyzing the long distance peaks in Fig. 6, we can observe that the peak for DMPC at gel phase is slightly narrower than that observed for the fluid phase, indicating the expected more restriction on the mobility of Laurdan and/or 2-TSC in the bilayer gel phase. Such mobility restriction is due to the greater lipid packaging in the gel phase than in the fluid phase.

Regarding the peaks associated to *cis* transfer, a significant increase in the contribution from closer pairs when the bilayer undergoes gel to fluid phase transition can be observed. There is also a small shift of the peak position to shorter distances: from 23.5 Å in the gel phase to 21.6 Å in the fluid phase. The decrease of the membrane rigidity allows a larger number of pairs to perform *cis* transfer over shorter distances.

Analyzing the intermediate peak, associated to *trans* transfer (Fig. 6): in the gel phase this peak has the greatest contribution, that is, a large number of pairs perform FRET at intermediate distances. Interestingly, in the fluid phase, with the increase in the fluidity of the bilayer, the population of the intermediate peak (*trans* transfer) is shift to the population associated with *cis* transfer and to the population associated with long distance FRET.

Fig. 8 shows the distribution of distances as a function of the concentration of acceptor in the system, for DMPC at the gel phase (panel A) and at the fluid phase (panel B).

As expected, at both gel and fluid phases, the increase in the concentration of 2-TSC favors the FRET to nearby acceptors, resulting in a strong decrease in the contribution of the long-distance peak. It is important to note that the results are very similar for the concentrations of 5 mol% and 10 mol%. That is, after saturation (Fig. 5) most of donor molecules undergo FRET to a nearby acceptor and there are too many acceptors in the system not performing FRET.

4. Conclusions

Here we discuss the quenching of the fluorescence signal of Laurdan by the thiosemicarbazone 2-TSC, both inserted into DMPC membranes, in the gel and fluid phases of the bilayer. A collisional quenching process was ruled out, due to the short lifetime of Laurdan and the diffusion coefficients of molecules in a lipid bilayer. On the other hand, the spectral overlap between the Laurdan fluo-

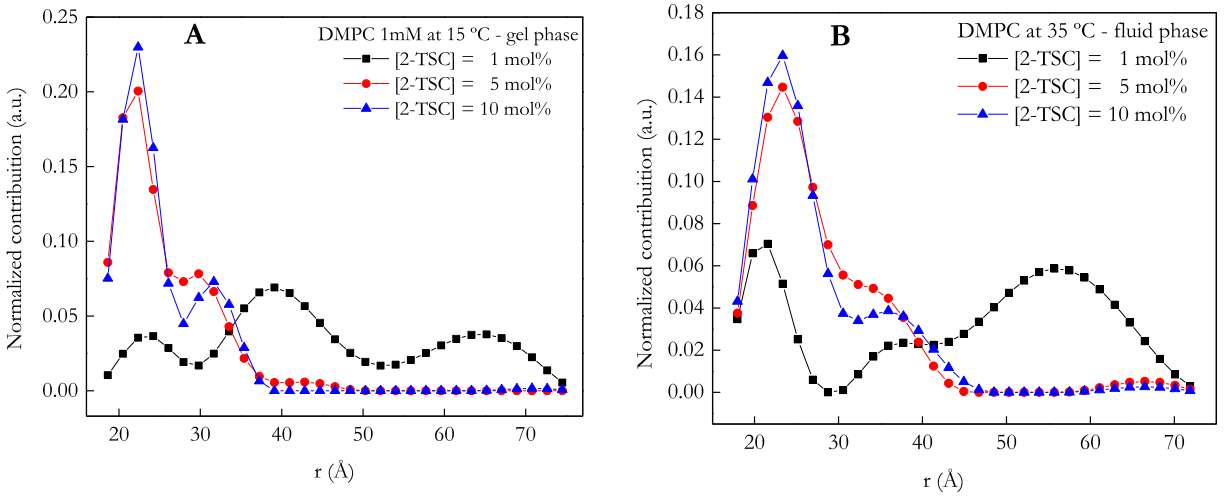

Fig. 8. Laurdan to 2-TSC distance distribution, obtained from fitting the FRET model to the Laurdan intensity decay data, in DMPC vesicles at 15 °C (A) and 35 °C (B) for the following concentrations of 2-TSC: 1 mol% (square), 5 mol% (circle) and 10 mol% (up triangle).

rescence spectrum and the 2-TSC absorption spectrum, although visually small, resulted in Förster distances of 37.2 Å and 35.9 Å, for the gel and fluid phases of the DMPC bilayer, respectively. Distance distributions between donor and acceptor groups were recovered using the program CONTIN, without other *a priori* assumptions regarding the shape of the distribution curves. The recovered distance distributions between naphthalene moiety of Laurdan and 2-TSC allowed the identification of donor–acceptor populations having different distances of separation. Moreover, it strongly supports the hypotheses of both molecules being localized close to the bilayer interface. The distance populations reflect the occurrence of FRET involving pairs donor/acceptor in the same leaflet of the lipid bilayer and pairs in opposite leaflet, and these results are in good agreement with our previous proposal about the lateral organization and position of Laurdan and 2-TSC molecules in a DMPC bilayer. A dynamic picture was obtained showing the changes in the relative position of the pairs dependent on the structural phase of the DMPC bilayer.

We show here that to identify the type of non-radiative probe deexcitation in lipid bilayers it is important to consider the fluorophore lifetimes and the diffusion coefficients of both the donor and the acceptor molecules.

CRediT authorship contribution statement

Cássia A. Marquezin: Data curation, Investigation, Project administration, Writing – original draft, Writing – review & editing. **M. Teresa Lamy:** Conceptualization, Funding acquisition, Writing – review & editing. **Eduardo S. de Souza:** Formal analysis, Writing – original draft, Writing – review & editing.

Declaration of Competing Interest

The authors declare that they have no known competing financial interests or personal relationships that could have appeared to influence the work reported in this paper.

Acknowledgment

M.T.L. is recipient of a CNPq research fellowship, and acknowledges the support of FAPESP (2017/25930-1; 2021/01593-1) and the National Institute of Science and Technology Complex Fluids (INCT-FCx), financed by CNPq (141260/2017-3) and FAPESP (2014/50983-3 and 2018/20162-9). The authors would like to thank one of the reviewers of the previous paper [43] for raising the subject discussed here. C.A.M. thanks UFG. E.S.S. thanks UFCAT. C.A.M., M.T.L. and E.S.S. thank Evandro L. Duarte and Cíntia C. Vequi-Suplicy for helping with the experiments and discussions.

References

[1] J.W. Lichtman, J.-A. Conchello, Fluorescence microscopy, Nat. Methods. 2 (12) (2005) 910–919, https://doi.org/10.1038/nmeth817.
[2] V.N. Mehta, M.L. Desai, H. Basu, R. Kumar Singhal, S.K. Kailasa, Recent developments on fluorescent hybrid nanomaterials for metal ions sensing and bioimaging applications: A review, J. Mol. Liq. 333 (2021) 115950, https://doi.org/10.1016/j.molliq.2021.115950.
[3] W. Quan, G. Zhang, L. Huang, W. Song, W. Lin, A novel fluorescent probe for high-fidelity imaging of mitochondria viscosity changes, J. Mol. Liq. 333 (2021) 115973, https://doi.org/10.1016/j.molliq.2021.115973.
[4] N.G. Ceffa, M. Bouzin, L. D'Alfonso, L. Sironi, C.A. Marquezin, F. Auricchio, S. Marconi, G. Chirico, M. Collini, Spatiotemporal Image Correlation Analysis for 3D Flow Field Mapping in Microfluidic Devices, Anal. Chem. 90 (3) (2018) 2277–2284, https://doi.org/10.1021/acs.analchem.7b04641.
[5] N.G. Ceffa, I. Cesana, M. Collini, L. D'Alfonso, S. Carra, F. Cotelli, L. Sironi, G. Chirico, Spatiotemporal image correlation analysis of blood flow in branched vessel networks of zebrafish embryos, J. Biomed. Opt. 22 (10) (2017) 1, https://doi.org/10.1117/1.JBO.22.10.106008.
[6] C.A. Marquezin, N.G. Ceffa, F. Cotelli, M. Collini, L. Sironi, G. Chirico, Image Cross-Correlation Analysis of Time Varying Flows, Anal. Chem. 88 (14) (2016) 7115–7122, https://doi.org/10.1021/acs.analchem.6b01143.
[7] V.M. Trusova, U.K. Tarabara, O.A. Zhytniakivska, K.O. Vus, G.P. Gorbenko, Probing the interactions of novel europium coordination complexes with serum albumin, Luminescence 36 (3) (2021) 795–801, https://doi.org/10.1002/bio.4006.
[8] M. Girych, G. Gorbenko, V. Trusova, E. Adachi, C. Mizuguchi, K. Nagao, H. Kawashima, K. Akaji, S. Lund-Katz, M.C. Phillips, H. Saito, Interaction of Thioflavin T with amyloid fibrils of apolipoprotein A-I N-terminal fragment: Resonance energy transfer study, J. Struct. Biol. 185 (1) (2014) 116–124, https://doi.org/10.1016/j.jsb:2013.10.017.
[9] J. Kaur, J.N. Malegaonkar, S.V. Bhosale, P.K. Singh, An anionic tetraphenyl ethylene based simple and rapid fluorescent probe for detection of trypsin and paraoxon methyl, J. Mol. Liq. 333 (2021) 115980, https://doi.org/10.1016/j.molliq.2021.115980.
[10] G. Gorbenko, V. Trusova, T. Deligeorgiev, N. Gadjev, C. Mizuguchi, H. Saito, Two-step FRET as a tool for probing the amyloid state of proteins, J. Mol. Liq. 294 (2019) 111675, https://doi.org/10.1016/j.molliq.2019.111675.
[11] U. Tarabara, E. Kirilova, G. Kirilov, K. Vus, O. Zhytniakivska, V. Trusova, G. Gorbenko, Benzanthrone dyes as mediators of cascade energy transfer in insulin amyloid fibrils, J. Mol. Liq. 324 (2021) 115102, https://doi.org/10.1016/j.molliq.2020.115102.
[12] J.R. Lakowicz, Principles of Fluorescense Spectroscopy, 3rd ed., Springer, Baltimore, USA, 2006.
[13] B. Valeur, Molecular Fluorescence (2001), https://doi.org/10.1002/3527600248.
[14] T. Förster, Intermolecular energy migration and fluorescence (Transl RS Knox), Ann. Phys. 2 (1948) 55–75.
[15] M. Stanisavljevic, S. Krizkova, M. Vaculovicova, R. Kizek, V. Adam, Quantum dots-fluorescence resonance energy transfer-based nanosensors and their application, Biosens. Bioelectron. 74 (2015) 562–574, https://doi.org/10.1016/j.bios.2015.06.076.
[16] Y. Rong, S. Ali, Q. Ouyang, L.i. Wang, B. Wang, Q. Chen, A turn-on upconversion fluorescence sensor for acrylamide in potato chips based on fluorescence resonance energy transfer and thiol-ene Michael addition, Food Chem. 351 (2021) 129215, https://doi.org/10.1016/j.foodchem.2021.129215.
[17] Y. Zhang, H. Xu, Y. Yang, F. Zhu, Y. Pu, X. You, X. Liao, Efficient fluorescence resonance energy transfer-based ratiometric fluorescent probe for detection of dopamine using a dual-emission carbon dot-gold nanocluster nanohybrid, J. Photochem. Photobiol. A Chem. 411 (2021) 113195, https://doi.org/10.1016/j.jphotochem.2021.113195.
[18] H. Yang, C. Hao, H. Liu, K. Zhong, R. Sun, Influence of bovine hemoglobin on the disruption of fluorescence resonance energy transfer between zinc sulfide quantum dots and fluorescent silica nanoparticles, J. Mol. Liq. 332 (2021) 115851, https://doi.org/10.1016/j.molliq.2021.115851.
[19] S. Nazerdeylami, J.B. Ghasemi, G. Mohammadi Ziarani, A. Amiri, A. Badiei, Direct monitoring of diclofenac using a supramolecular fluorescent approach based on β-cyclodextrin nanosponge, J. Mol. Liq. 336 (2021) 116104, https://doi.org/10.1016/j.molliq.2021.116104.
[20] A.F. Sierra, D. Hernández-Alonso, M.A. Romero, J.A. González-Delgado, U. Pischel, P. Ballester, Optical Supramolecular Sensing of Creatinine, J. Am. Chem. Soc. 142 (9) (2020) 4276–4284, https://doi.org/10.1021/jacs.9b12071.
[21] A.J.P. Teunissen, C. Pérez-Medina, A. Meijerink, W.J.M. Mulder, Investigating supramolecular systems using Förster resonance energy transfer, Chem. Soc. Rev. 47 (18) (2018) 7027–7044, https://doi.org/10.1039/C8CS00278A.
[22] M. Bood, S. Sarangamath, M.S. Wranne, M. Grøtli, L.M. Wilhelmsson, Fluorescent nucleobase analogues for base–base FRET in nucleic acids: synthesis, photophysics and applications, Beilstein J. Org. Chem. 14 (2018) 114–129, https://doi.org/10.3762/bjoc.14.7.
[23] S.C.Y. Jeng, R.J. Trachman, F. Weissenboeck, L. Truong, K.A. Link, M.D.E. Jepsen, J.R. Knutson, E.S. Andersen, A.R. Ferré-D'Amaré, P.J. Unrau, Fluorogenic aptamers resolve the flexibility of RNA junctions using orientation-dependent FRET, RNA 27 (4) (2021) 433–444, https://doi.org/10.1261/rna.078220.120.
[24] Y. Kamiya, H. Kamimoto, H. Zhu, H. Asanuma, Development and Modification of Pre-miRNAs with a FRET Dye Pair for the Intracellular Visualization of Processing Intermediates That Are Generated in Cells, Sensors. 21 (2021) 1785, https://doi.org/10.3390/s21051785.
[25] A. Megalathan, K.M. Wijesinghe, S. Dhakal, Single-Molecule FRET-Based Dynamic DNA Sensor, ACS Sensors 6 (3) (2021) 1367–1374, https://doi.org/10.1021/acssensors.1c00002.
[26] A. Siuiti Ito, E. Sérgio de Souza, S. dos Reis Barbosa, C. Ryuichi Nakaie, Fluorescence study of conformational properties of melanotropins labeled with aminobenzoic acid, Biophys. J. 81 (2) (2001) 1180–1189, https://doi.org/10.1016/S0006-3495(01)75775-X.
[27] L.R. Montaldi, M. Berardi, E.S. Souza, L. Juliano, A.S. Ito, End-to-end Distance Distribution in Fluorescent Derivatives of Bradykinin in Interaction with Lipid Vesicles, J. Fluoresc. 22 (4) (2012) 1151–1158, https://doi.org/10.1007/s10895-012-1054-0.
[28] E.S. de Souza, A.H. Katagiri, L. Juliano, M.A. Juliano, D.C. Pimenta, A.S. Ito, Fret studies of conformational changes in heparin-binding peptides, J. Fluoresc. 24 (3) (2014) 885–894, https://doi.org/10.1007/s10895-014-1366-3.

[29] A. Synak, R. Fudala, I. Gryczynski, L. Kułak, S. Shah, I.E. Serdiuk, B. Grobelna, P. Arłukowicz, A. Kubicki, P. Bojarski, AMCA to TAMRA long range resonance energy transfer on a flexible peptide, Dye. Pigment. 158 (2018) 60–64, https://doi.org/10.1016/j.dyepig.2018.05.019.
[30] L.M.S. Loura, A. Fedorov, M. Prieto, Fluid-Fluid Membrane Microheterogeneity: A Fluorescence Resonance Energy Transfer Study, Biophys. J. 80 (2) (2001) 776–788, https://doi.org/10.1016/S0006-3495(01)76057-2.
[31] L. Loura, M. Prieto, FRET in membrane biophysics: an overview, Front. Physiol. 2 (2011), https://doi.org/10.3389/fphys.2011.00082.
[32] D.S. Tretiakova, A.S. Alekseeva, T.R. Galimzyanov, A.M. Boldyrev, A.Y. Chernyadyev, Y.A. Ermakov, O.V. Batishchev, E.L. Vodovozova, I.A. Boldyrev, Lateral stress profile and fluorescent lipid probes. FRET pair of probes that introduces minimal distortions into lipid packing, Biochim. Biophys. Acta - Biomembr. 1860 (11) (2018) 2337–2347, https://doi.org/10.1016/j.bbamem.2018.05.020.
[33] L. Loura, Lateral Distribution of NBD-PC Fluorescent Lipid Analogs in Membranes Probed by Molecular Dynamics-Assisted Analysis of Förster Resonance Energy Transfer (FRET) and Fluorescence Quenching, Int. J. Mol. Sci. 13 (2012) 14545–14564, https://doi.org/10.3390/ijms131114545.
[34] M.K. Singh, M.F. Khan, H. Shweta, S. Sen, Probe-location dependent resonance energy transfer at lipid/water interfaces: comparison between the gel- and fluid-phase of lipid bilayer, Phys. Chem. Chem. Phys. 19 (38) (2017) 25870–25885, https://doi.org/10.1039/C7CP03108D.
[35] T.A. Enoki, F.A. Heberle, G.W. Feigenson, FRET Detects the Size of Nanodomains for Coexisting Liquid-Disordered and Liquid-Ordered Phases, Biophys. J. 114 (8) (2018) 1921–1935, https://doi.org/10.1016/j.bpj.2018.03.014.
[36] C.A. Marquezin, A.S. Ito, E.S. de Souza, Organization and dynamics of NBD-labeled lipids in lipid bilayer analyzed by FRET using the small membrane fluorescent probe AHBA as donor, Biochim. Biophys. Acta - Biomembr. 1861 (10) (2019) 182995, https://doi.org/10.1016/j.bbamem.2019.05.017.
[37] W. Saeed, Z. Abbasi, S. Majeed, S.A. Shahzad, A.F. Khan, A.J. Shaikh, An insight into the binding behavior of graphene oxide and noble metal nanoparticles, J. Appl. Phys. 129 (12) (2021) 125302, https://doi.org/10.1063/5.0041894.
[38] S.K. Vaishanav, J. Korram, R. Nagwanshi, I. Karbhal, L. Dewangan, K.K. Ghosh, M.L. Satnami, Interaction of Folic Acid with Mn2+ Doped CdTe/ZnS Quantum Dots. In Situ Detection of Folic Acid, J. Fluoresc. 31 (4) (2021) 951–960, https://doi.org/10.1007/s10895-021-02708-1.
[39] J. Aslam, I. Hussain Lone, F. Ansari, A. Aslam, R. Aslam, M. Akram, Molecular binding interaction of pyridinium based gemini surfactants with bovine serum albumin: Insights from physicochemical, multispectroscopic, and computational analysis, Spectrochim. Acta Part A Mol. Biomol. Spectrosc. 250 (2021) 119350, https://doi.org/10.1016/j.saa.2020.119350.
[40] M. Mathew, T.V. Divyalakshmi, C.T. Aravindakumar, U.K. Aravind, Potential involvement of environmental triggers in protein aggregation with mercuric chloride as a model, Int. J. Biol. Macromol. 174 (2021) 153–161, https://doi.org/10.1016/j.ijbiomac.2021.01.134.
[41] A.P. Romani, C.A. Marquezin, A.S. Ito, Fluorescence spectroscopy of small peptides interacting with microheterogeneous micelles, Int. J. Pharm. 383 (1-2) (2010) 154–156, https://doi.org/10.1016/j.ijpharm.2009.09.017.
[42] A.P. Romani, C.A. Marquezin, A.E.E. Soares, A.S. Ito, Study of the interaction between apis mellifera venom and micro-heterogeneous systems, J. Fluoresc. 16 (3) (2006) 423–430, https://doi.org/10.1007/s10895-006-0077-9.
[43] C.A. Marquezin, C.M.A. de Oliveira, F. Vandresen, E.L. Duarte, M.T. Lamy, C.C. Vequi-Suplicy, The interaction of a thiosemicarbazone derived from R - (+) - limonene with lipid membranes, Chem. Phys. Lipids. 234 (2021) 105018, https://doi.org/10.1016/j.chemphyslip.2020.105018.
[44] F. Vandresen, H. Falzirolli, S.A. Almeida Batista, A.P.B. da Silva-Giardini, D.N. de Oliveira, R.R. Catharino, A.L.T.G. Ruiz, J.E. de Carvalho, M.A. Foglio, C.C. da Silva, Novel R-(+)-limonene-based thiosemicarbazones and their antitumor activity against human tumor cell lines, Eur. J. Med. Chem. 79 (2014) 110–116, https://doi.org/10.1016/j.ejmech.2014.03.086.
[45] L. Alonso, C.A. Marquezin, P.J. Gonçalves, A. Alonso, Transmittance and Autofluorescence of Neonatal Rat Stratum Corneum: Nerolidol Increases the Dynamics and Partitioning of Protoporphyrin IX into Intercellular Membranes, J. Fluoresc. 26 (2) (2016) 709–717, https://doi.org/10.1007/s10895-015-1758-z.
[46] S.A. Mendanha, C.A. Marquezin, A.S. Ito, A. Alonso, Effects of nerolidol and limonene on stratum corneum membranes: A probe EPR and fluorescence spectroscopy study, Int. J. Pharm. 532 (1) (2017) 547–554, https://doi.org/10.1016/j.ijpharm.2017.09.046.
[47] C.C. Vequi-Suplicy, M.T. Lamy, C.A. Marquezin, The new fluorescent membrane probe Ahba: A comparative study with the largely used Laurdan, J. Fluoresc. 23 (2013) 479–486, https://doi.org/10.1007/s10895-013-1172-3.
[48] M.A. Soto-Arriaza, C. Olivares-Ortega, F.H. Quina, L.F. Aguilar, C.P. Sotomayor, Effect of cholesterol content on the structural and dynamic membrane properties of DMPC/DSPC large unilamellar bilayers, Biochim. Biophys. Acta - Biomembr. 1828 (11) (2013) 2763–2769, https://doi.org/10.1016/j.bbamem.2013.07.031.
[49] C.C. Vequi-Suplicy, K. Coutinho, M.T. Lamy, Electric dipole moments of the fluorescent probes Prodan and Laurdan: experimental and theoretical evaluations, Biophys. Rev. 6 (1) (2014) 63–74, https://doi.org/10.1007/s12551-013-0129-8.
[50] S.S.W. Leung, J. Brewer, L.A. Bagatolli, J.L. Thewalt, Measuring molecular order for lipid membrane phase studies: Linear relationship between Laurdan generalized polarization and deuterium NMR order parameter, Biochim. Biophys. Acta - Biomembr. 1861 (12) (2019) 183053, https://doi.org/10.1016/j.bbamem.2019.183053.
[51] I.R. Calori, W.M. Pazin, K. Brunaldi, D.S. Pellosi, W. Caetano, A.C. Tedesco, N. Hioka, Laurdan as fluorescent probe to determinate the critical micelle temperature of polymers from Pluronic®-coated fluid phase liposomes, J. Mol. Liq. 294 (2019) 111562, https://doi.org/10.1016/j.molliq.2019.111562.
[52] S. Osella, N. Smisdom, M. Ameloot, S. Knippenberg, Conformational Changes as Driving Force for Phase Recognition: The Case of Laurdan, Langmuir 35 (35) (2019) 11471–11481, https://doi.org/10.1021/acs.langmuir.9b01840.
[53] M.K. Masukawa, C.C. Vequi-Suplicy, E.L. Duarte, M.T. Lamy, A closer look into laurdan as a probe to monitor cationic DODAB bilayers, J. Photochem. Photobiol. A Chem. 376 (2019) 238–246, https://doi.org/10.1016/j.jphotochem.2019.03.006.
[54] F.S. Pessoto, C.H. Yokomizo, T. Prieto, C.S. Fernandes, A.P. Silva, C.R. Kaiser, E.A. Basso, I.L. Nantes, Thiosemicarbazone p -Substituted Acetophenone Derivatives Promote the Loss of Mitochondrial Δ ψ, GSH Depletion, and Death in K562 Cells, Oxid. Med. Cell. Longev. 2015 (2015) 1–15, https://doi.org/10.1155/2015/394367.
[55] Cíntia.C. De Vequi-Suplicy, C.R. Benatti, M.T. Lamy, Laurdan in Fluid Bilayers: Position and Structural Sensitivity, J. Fluoresc. 16 (3) (2006) 431–439, https://doi.org/10.1007/s10895-005-0059-3.
[56] V.M. Trusova, G.P. Gorbenko, Membrane interactions of fibrillar lysozyme: Effect of lipid bilayer composition, J. Mol. Liq. 274 (2019) 338–344, https://doi.org/10.1016/j.molliq.2018.10.103.
[57] S.W. Provencher, CONTIN: A general purpose constrained regularization program for inverting noisy linear algebraic and integral equations, Comput. Phys. Commun. 27 (3) (1982) 229–242, https://doi.org/10.1016/0010-4655(82)90174-6.
[58] M.J. Hope, M.B. Bally, G. Webb, P.R. Cullis, Production of large unilamellar vesicles by a rapid extrusion procedure. Characterization of size distribution, trapped volume and ability to maintain a membrane potential, BBA - Biomembr. 812 (1) (1985) 55–65, https://doi.org/10.1016/0005-2736(85)90521-8.
[59] D.C. Pimenta, I.L. Nantes, E.S. De Souza, B. Le Bonniec, A.S. Ito, I.L.S. Tersariol, V. Oliveira, M.A. Juliano, L. Juliano, Interaction of heparin with internally quenched fluorogenic peptides derived from heparin-binding consensus sequences, kallistatin and anti-thrombin III, Biochem. J. 366 (2002), https://doi.org/10.1042/BJ20020023.
[60] E.S. De Souza, I.Y. Hirata, L. Juliano, A.S. Ito, End-to-end distance distribution in bradykinin observed by Forster resonance energy transfer, Biochim. Biophys. Acta - Gen. Subj. 1474 (2000) 251–261, https://doi.org/10.1016/S0304-4165(00)00004-0.
[61] B.A. Rowe, S.L. Neal, Photokinetic analysis of PRODAN and LAURDAN in large unilamellar vesicles from multivariate frequency-domain fluorescence, J. Phys. Chem. B. 110 (30) (2006) 15021–15028, https://doi.org/10.1021/jp036664n.
[62] C.C. Vequi-Suplicy, K. Coutinho, M.T. Lamy, New Insights on the Fluorescent Emission Spectra of Prodan and Laurdan, J. Fluoresc. 25 (3) (2015) 621–629, https://doi.org/10.1007/s10895-015-1545-x.
[63] C.C. Vequi-Suplicy, Y. Orozco-Gonzalez, M.T. Lamy, S. Canuto, K. Coutinho, A new interpretation of the absorption and the dual fluorescence of Prodan in solution, J. Chem. Phys. 153 (24) (2020) 244104, https://doi.org/10.1063/5.0025013.
[64] A.D. Lúcio, Cíntia.C. Vequi-Suplicy, R.M. Fernandez, M.T. Lamy, Laurdan spectrum decomposition as a tool for the analysis of surface bilayer structure and polarity: A study with DMPG, peptides and cholesterol, J. Fluoresc. 20 (2) (2010) 473–482, https://doi.org/10.1007/s10895-009-0569-5.
[65] D. Ionescu, C. Ganea, A study of quercetin effects on phospholipid membranes containing cholesterol using Laurdan fluorescence, Eur. Biophys. J. 41 (3) (2012) 307–318, https://doi.org/10.1007/s00249-011-0786-0.
[66] D. Marsh, Handbook of lipids bilayers, CRC, Boca Raton, 1990.
[67] J. Katsaras, T. Gutberlet (Eds.), Lipid Bilayers, Springer Berlin Heidelberg, Berlin, Heidelberg, 2001.
[68] M. Lúcio, C. Nunes, D. Gaspar, K. Gołębska, M. Wisniewski, J.L.F.C. Lima, G. Brezesinski, S. Reis, Effect of anti-inflammatory drugs in phosphatidylcholine membranes: A fluorescence and calorimetric study, Chem. Phys. Lett. 471 (4-6) (2009) 300–309, https://doi.org/10.1016/j.cplett.2009.02.047.
[69] H. Kautsky, Quenching of luminescence by oxygen, Trans. Faraday Soc. 35 (1939) 216, https://doi.org/10.1039/tf9393500216.
[70] V.K. Sharma, E. Mamontov, M. Tyagi, S. Qian, D.K. Rai, V.S. Urban, Dynamical and Phase Behavior of a Phospholipid Membrane Altered by an Antimicrobial Peptide at Low Concentration, J. Phys. Chem. Lett. 7 (2016), https://doi.org/10.1021/acs.jpclett.6b01006.
[71] M. Jan Akhunzada, F. D'Autilia, B. Chandramouli, N. Bhattacharjee, A. Catte, R. Di Rienzo, F. Cardarelli, G. Brancato, Interplay between lipid lateral diffusion, dye concentration and membrane permeability unveiled by a combined spectroscopic and computational study of a model lipid bilayer, Sci. Rep. 9 (1) (2019), https://doi.org/10.1038/s41598-018-37814-x.
[72] J.R. Silvius, I.R. Nabi, Fluorescence-quenching and resonance energy transfer studies of lipid microdomains in model and biological membranes (review), Mol. Membr. Biol. 23 (1) (2006) 5–16, https://doi.org/10.1080/09687860500473002.
[73] Lakowicz, F. Prendergast, Quantitation of hindered rotations of diphenylhexatriene in lipid bilayers by differential polarized phase fluorometry, Science (80-.) 200 (4348) (1978) 1399–1401, https://doi.org/10.1126/science:663620.

[74] A. Synak, P. Bojarski, M. Sadownik, L. Kułak, I. Gryczynski, B. Grobelna, S. Rangełowa-Jankowska, D. Jankowski, A. Kubicki, Excitation energy transfer in partly ordered polymer films differing in donor and acceptor transition moments orientation, Opt. Mater. (Amst) 59 (2016) 34–38, https://doi.org/10.1016/j.optmat.2016.03.005.

[75] S. Tristram-Nagle, Y. Liu, J. Legleiter, J.F. Nagle, Structure of gel phase DMPC determined by x-ray diffraction, Biophys. J. 83 (6) (2002) 3324–3335, https://doi.org/10.1016/S0006-3495(02)75333-2.

[76] J.F. Nagle, S. Tristram-Nagle, Structure of lipid bilayers, Biochim. Biophys. Acta - Rev. Biomembr. 1469 (3) (2000) 159–195, https://doi.org/10.1016/S0304-4157(00)00016-2.